Non-Interceptive Beam Current and Position Monitors for a Cyclotron Based Proton Therapy Facility

Srinivasan, Sudharsan

DOI:
10.33612/diss.149817352

Chapter 1: Introduction

1.1 Radiation therapy

Cancer therapies have the objective to remove or destroy cancerous tissues (tumors) with limited damage to healthy organs. Typically, the treatment of tumors is a multimodality approach [1], which includes surgery, chemotherapy, radiation, and immunotherapy. For any treatment modality, when there is no recurrence of the same tumor type at the same location within five years, the cancer is considered to be cured.

Radiation therapy is a treatment method for well-localized tumors, where the dose delivered should be as conformal as possible. This is to ensure the tumor tissue gets a high radiation dose with surrounding healthy tissues receiving as low dose as possible. This demands a precise administration of the dose.

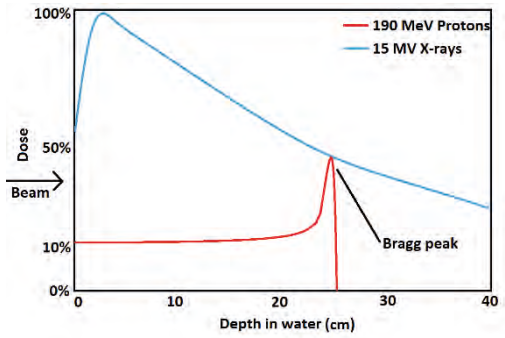

Figure 1.1: Depth-dose distributions from a monoenergetic photon beam (15 MV) and a monoenergetic proton beam (190 MeV) [2]. The beam enters from the left. For photons, the maximum dose is close to the entrance and decreases with depth. For the protons, the dose depth is characterized by the deposition of maximum energy per path length close to the end of the range, given by the Bragg peak.

Proton radiation therapy has its depth-dose distribution characterized by a well-defined peak, called Bragg peak [3], as shown in Figure 1.1. In this peak, protons stop and deposit their maximum dose, beyond which the dose falls to zero within millimeters. Because of the Bragg peak nature, the dose deposition can be highly localized within the tumor volume, and the dose delivered to the healthy tissues can be strongly reduced as compared to that in conventional radiotherapy. Also,

in the lateral direction, proton beams give a sharply bounded dose distribution. In order to be sure that the dose is delivered correctly, the beam current and its position have to be carefully prepared. To achieve this, reliable and accurate beam diagnostics are needed in the beam transport system. Using a well-controlled beam, protons offer more flexibility in administering the dose distribution as compared to photons. Furthermore, the total energy deposited is at least a factor three lower than photon therapy [1].

However, the higher costs associated with proton therapy, as compared to conventional radiation therapy, is possibly the reason for the limited clinical adoption of proton therapy.

Paul Scherrer Institut (PSI) has a radiation therapy facility PROSCAN [4], which is using proton beams. Here one uses the irradiation technique called spot scanning, which is able to deliver dose accurately to the shape of the tumor, which is generally irregular.

1.2 PROSCAN: COMET, its beamlines and diagnostics

The PROSCAN project was initiated at the Paul Scherrer Institut in 2000 with the objective to develop the PSI Spot-Scanning technology in a hospital environment [4]. The PROSCAN facility consists of a dedicated 250 MeV cyclotron, followed by a degrader and energy selection system splitting into multiple beamlines that lead to therapy machinery (gantries, eye-treatment facility) and an experimentation beamline. A brief description of the constituents of the PROSCAN is given below.

1.2.1 COMET cyclotron

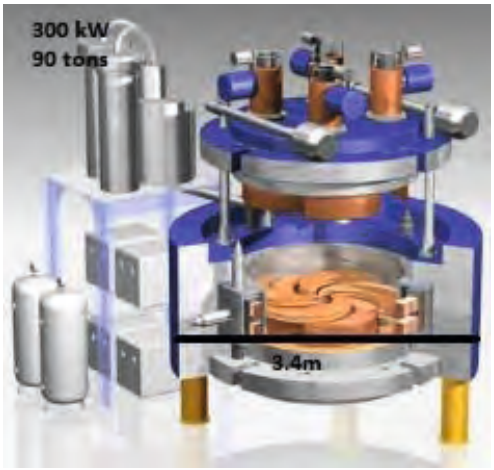

Figure 1.2: Schematic representation of the COMET cyclotron. Mentioned are the power consumption, its weight, and external diameter [4].

The COMET cyclotron was manufactured by ACCEL Instruments in collaboration with PSI based on the design of H. Blosser *et al.* [5]. The cyclotron, whose magnetic field is produced by a set of superconducting coils, delivers a continuous wave proton beam with an energy of 250 MeV. Thanks to the superconducting magnet, the COMET is a compact system that reliably delivers a beam with all-year-round availability. A Schematic of the COMET is shown in Figure 1.2, with its key parameters listed in the Appendix (1TA 1).

1.2.2 Degrader

Since the cyclotron delivers a proton beam with a single, fixed energy, the energy modulation of the proton beam required for proton therapy is produced with a variable thickness carbon-wedge degrader in the beamline. The degrader is an assembly of a pair of multiple wedges providing an energy setting in the range of 238-70 MeV. The degrader is mounted in a vacuum chamber, which is also equipped with beam current monitors, beam profile monitors, a beam stopper before the degrader, and a beam size defining collimator after the degrader [6]. The schematic layout of the degrader is shown in Figure 1.3. Following the degrader, the beam is guided to the treatment rooms through multiple beamlines, as shown in Figure 1.4.

Figure 1.3: The carbon-wedge degrader unit consisting of its diagnostics, a beam stopper, pair of multi-wedges, and a collimator system [4].

1.3 PROSCAN beam diagnostics

PROSCAN incorporates checkpoints to comply with the safe operation of the beam that is based on verification of certain beam parameters such as current, position, energy, etc. In the PROSCAN facility, the control and monitoring of the beam parameters are performed with several beam diagnostic elements [7]. The beam current plays a critical role as it is directly linked to the dose-rate applied to the patient. Therefore, it requires accurate and precise determination during standard operation [8]. This puts a demand on the diagnostics to deliver highly accurate signals with minimum beam disturbance [9].

The beam current, which is in the range of 0.1-10 nA, is monitored by ionization chambers (ICs) and secondary emission monitors. Their default state (i.e., in or out of the beamline) depends on the thickness of these monitors (thick and thin monitors). For instance, the presence of a thick monitor in the beamline during patient treatment will trigger the interlocks of the transmission verification system [4]. For error detection, halo monitors (ICs) provide reliable measurements of the beam position. A multi-layer Faraday cup (FC) inserted in the beamline provides fast measurements of the beam energy and momentum spread [10].

Detailed information on the performance and limitations of the above-mentioned monitors can be found in [11]–[14].

1.3.1 Drawbacks of the existing diagnostics

Some of the beam diagnostics in PROSCAN continuously monitor the previously mentioned parameters as a safety measure. These measurements are performed with thin profile monitors to prevent excessive multiple scattering [7], which would compromise the beam quality. Moreover, the current dependent

recombination effects from these monitors should be less than 5%. However, for small beam diameters, the recombination effects become dominant for higher beam currents. Due to the associated multiple scattering issues, the thin monitors also will increase the beam emittance [13].

The thick monitors have the drawback of afterglow problems due to activation. Moreover, the insertion of these monitors during operation could result in eigenmode excitations of the foils, which could lead to microphonic noise by nearby moving actuators. Experience shows that this microphonic noise could be up to 0.2 $nA_{peak\text{-}peak}$ equivalent signal at 1 kHz, while in Secondary Emission Monitors (SEMs), the microphonic noise could account even up to 25 $nA_{peak\text{-}peak}$ from noise due to mechanical vibrations. Driving the degrader actuator alongside increases this noise level to 60 $nA_{peak\text{-}peak}$.

For beam loss measurements at the coupling points of the gantries to the beamline, the halo monitors provide a beam current resolution of 10 pA with the lowest-detection threshold ion in the order of 0.1 nA, at the expense of new halo generation and scattering, especially at higher beam currents [12], [13].

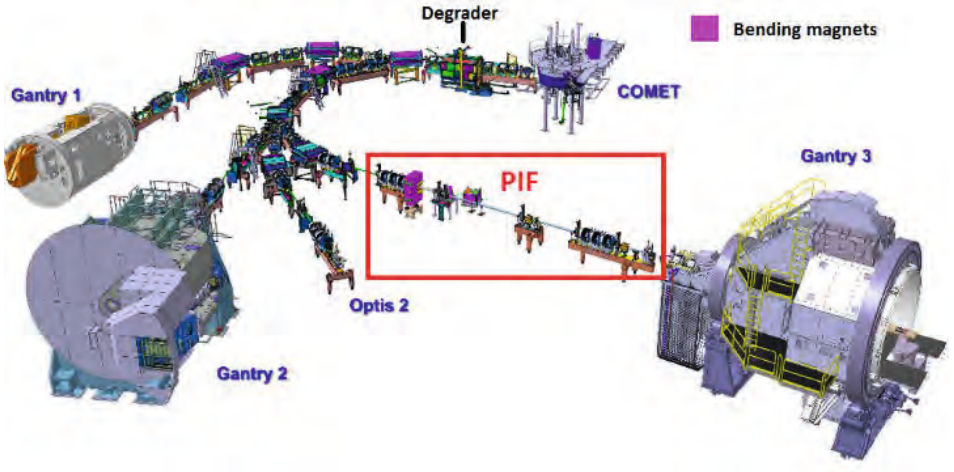

Figure 1.4: PSI PROSCAN layout. Multiple beamlines after degrader lead to multiple gantries (1,2 and 3). Optis 2 is dedicated to ocular tumor treatment. The red highlighted area represents the Proton Irradiation Facility (PIF).

1.4 Beam diagnostic measurement specifications for PROSCAN

The PROSCAN facility provides to the user a beam with specified characteristics. At certain checkpoints in the beamlines the user verifies these specified characteristics of the beam with the aid of diagnostics, namely current, position,

and energy. The diagnostics at certain locations such as those in front of the degrader, at the checkpoint before the gantry (i.e., coupling points), and the beam stoppers (FCs) constitute the most important diagnostics of the beamline [11]. The beam current brought to the gantries, generally in the range of (0.1-10 nA), needs to be measured accurately with minimal disturbance. These invasive monitors, susceptible to multiple Coulomb scattering and inelastic nuclear scattering, causes the beam to broaden.

A maximum beam current of 10 nA in the energy range of 230 MeV – 70 MeV [7].can be delivered to the therapy machinery (i.e., the gantries). Since the beam current and its position have a direct correlation to the quality of the applied dose distribution, there is a demand to measure the beam parameters accurately with minimal beam disturbances. Therefore, a detection threshold of 0.1 nA with a resolution of 50 pA is required at low beam currents. Similarly, the position resolution for the beam position should be better than 0.5 mm.

1.5 Parameters of Interest: Beam Current and Beam Position

This thesis deals with the non-intercepting measurement of beam current and position. On that account, a brief description of these beam parameters serves as a basis for the comfort of the reader.

During the standard operation of a particle accelerator, the beam current is one of the most important parameters to be measured. Usually, beam current (number of protons per second) is expressed as an electric current (A). Different terminologies are expressing the time structure of the used beam, shown in Figure 1.5. These are:

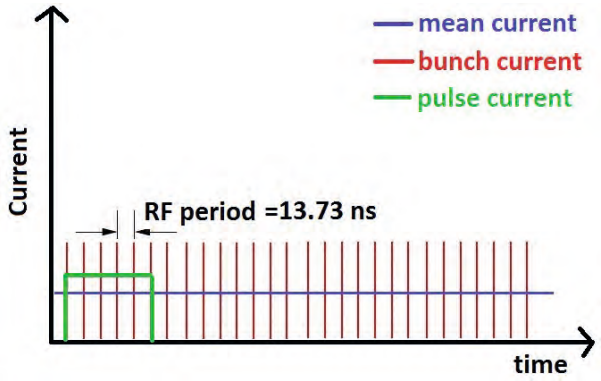

Figure 1.5: The time structure of different currents from a pulsed beam structure [15].

- The mean current I_{mean} represents the long time average (units of A)
- The pulse current I_{pulse} is the time average while the beam is on (units of A)
- The bunch current I_{bunch} represents the instantaneous beam current (units of A), which is very high as it is concentrated in a very short time.

COMET is a continuous wave (CW) accelerator; it delivers bunches continuously at a high RF frequency of 72.85 MHz. A non-periodic macro pulse structure, 10-1000 Hz, will be present in the beam transport system when the spot scanning procedure (beam delivery) is applied at the treatment. Due to the CW character of the continuous RF acceleration by the cyclotron [15], the I_{pulse} equates $I_{mean,}$ with no alteration in the bunch structure.

The next parameter of interest, beam position, is the information on the position of the centroid of the beam within the vacuum chamber [16]. For the transfer lines from the COMET to the gantries, the beam position information helps to measure and correct beam trajectories. Generally, the position information of the beam relates to the (X, Y) coordinate, where X = Y = 0 represents the axis of the beam transport system and X = horizontal (+ = right) and Y = vertical (+ = up).

Both these parameters are traditionally measured with interceptive monitors, as discussed in section 1.3. A brief description of their working principle is given below.

1.6 Interceptive Beam Diagnostics

At PROSCAN, the most commonly used beam diagnostics are FCs, ICs, and SEMs, as discussed before in section 1.3. A brief review of their characterization is given below. More information is presented in [15], [17].

1.6.1 Faraday cups (FCs)

The simplest way to measure beam current is by capturing it and reading it with a current meter. Technically, an FC is a beam stopper connected to a sensitive pre-amplifier. Especially for lower beam currents down to even a few pA [15], measurements have been successfully performed with Faraday cups. With a careful mechanical design, this measurement is five orders of magnitude more sensitive than a sensitive dc current transformer [18]. One of the major concerns is the event of backscattered particles (mostly electrons from secondary emission following the proton interactions) that may escape, which then demands a design of a narrow cup entrance and/or a ring at negative high voltage. Another concern

is the power of the spent beam that can affect the stability of the measurement, which can be mitigated by effective cooling. Faraday cups used for high beam currents can be found in [15].

1.6.2 Ionization chambers (ICs)

For medium current ranges from 10^4 to 10^9 particles per second, the beam current is best determined by the ionization it produces in a gas-filled chamber [15]. Along the trajectory of a proton, a number of electron-ion pairs are produced due to the ionization of molecules of the gases inside the ionization chamber [15]. In most cases, nitrogen, air, or pure argon is used, where the active gas volume is confined between two metalized plastic foils. The thickness of the foils is an important consideration in the design of ICs as they determine the amount of energy loss in them. The measured ionization current primarily depends on the number of incident beam particles as well as their energy. For energies lower than approximately 1 GeV/u, the energy loss per nucleon is strongly dependent on the energy; thus, it is necessary to know the beam energy for high accuracy beam current measurements. The lower detection threshold of the ionization chamber is a beam current of 1 pA [19], thus making it a suitable choice for low current measurements, however, with some associated issues as mentioned in subsection 1.3.1.

1.6.3 Secondary Emission Monitors (SEMs)

For current ranges beyond 10^8 particles per second, predominantly SEMs are used, which measure the yield of secondary electrons emitted from a metallic foil inserted in the beam. The setup consists of three metallic foils, mostly around 100 μm thick Al-foils. The outer two foils are biased at 100 V to sweep away the free electrons towards the middle foil that is connected to a sensitive amplifier [15]. The secondary emission, given by the Sternglass formula [20], demands an experimental calibration prior to the measurement to obtain a high accuracy value of the secondary electron emission coefficient. The actual value of the secondary electron emission coefficient is also dependent on the surface structure of the material, thus affecting the accuracy depending on the production and cleaning methods of the foil. Radiation hardness of the foil material is important, as they are most often inserted in the beam because material degradation will change the secondary electron emission coefficient.

1.7 Non-interceptive beam diagnostics

In the previous section, we have reviewed the working principle of the most dominantly used beam diagnostics in PROSCAN. In this section, we review the non-interceptive beam diagnostic techniques that are conventionally used in particle accelerator facilities for the measurement of beam current and position. Cited along are their detection threshold, drawbacks, and supplementary recommendations for their efficient usage. Most of the non-interceptive beam current or position monitors employ either the electric or the magnetic field created by the passing charged particle beam for detection [21].

More detailed information on the principle of operation and limitations of the monitors mentioned can be found in [22].

1.7.1 Beam Current Transformers (BCTs)

Beam current transformers (BCTs) couple to the magnetic field of a charged particle beam. The magnetic field induced by the beam current at a particular point is given by the Biot-Savart law [23]. The schematic setup of a beam current transformer [15] is to pass the beam, which acts as the primary winding through a ferrite torus around which an insulated wire is wound that acts as the secondary winding with a given inductance. The torus guides the magnetic field lines of the beam such that only the azimuthal component is measured, thus making the measurement position-independent. The design criteria of a BCT are given in detail in [15]. The BCTs are used only for pulsed beams since they are only sensitive to changes in the B-field flux. Passive transformers are used only for beam pulse length between 1 ns and 10 μs. Active transformers find their use for beam pulse length longer than 10 μs. Most of the BCTs are not suitable for the measurement of low current charge particle beams due to their detection threshold limit of ~100 μA [24]. Moreover, at higher frequencies, they are sensitive to both beam position and bunch length, thus affecting signal sensitivity. Integrated Current Transformers such as at the National Synchrotron Light Source – II (NSLS-II) facility [25] and also from Bergoz Instrumentation [26] have demonstrated better signal sensitivity than conventional BCTs. However, the pulse charge should be at least a few pC.

1.7.2 Capacitive monitors

For beam current and position measurements of low bunch charges, capacitive monitors, which couple to the electric field of the charged particle beam, might be a practical solution. These capacitive monitors are constructed as opposing

metallic electrodes within the beam pipe such that their difference in the signal provides position information, and summation of their signals provides beam current information. Linear-cut or shoe-box capacitive monitors find their use where the frequency of the charged particle bunch is less than 10 MHz [22]. For frequencies higher than 10 MHz and up to 3 GHz, button monitors are the preferred choice due to their compact installation. For instance, button monitors in the Argonne Wakefield Accelerator (AWA) have demonstrated a detection threshold of the button monitors down to 100 *fC* [27]. Stripline monitors that are more suited for short bunches provide higher position and time resolution of the signal due to higher azimuthal coverage of the beam at the expense of more complex mechanical realization [28].

1.7.3 Wall Current Monitors (WCMs)

The wall current or image current is the representation of the beam image with no dc component. Similar to the beam, the wall current is an ideal current source with infinite output impedance. Thus, measuring this current across a resistor, as in the case of resistive wall current monitors, provides a measurable voltage. The resistors are in general constructed in parallel such that the total resistance is typically 1 Ω. Resistive WCMs are limited by their high detection threshold as at Injecteur de Protons à Haute Intensité (IPHI) in Saclay [29]. Similar to the resistive WCMs, inductive WCMs, which employ inductive pickups sensing the azimuthal distribution of the image current, is limited by parasitic inductance as in CLIC Test Facility 3 Drive Beam Linac (CTF3 DBL) [30]. These WCMs (both resistive and inductive) have bandwidth limitations that can be improved by placing ferrite cores as recommended by [31], [32]. WCMs are also limited in performance due to wakefield contamination, which requires a microwave absorber as implemented in the Fermilab Tevatron project [33].

1.7.4 Cavity resonators

Cavity resonators have shown to be suitable for beam intensities in the range of a few nA and when beam bunches are shorter than 1 μs. These monitors can measure a position with high-resolution demands [34], and as they can provide information even without the need for averaging possibilities. The requirement for high resolution and low detection threshold is achieved by the excitation of TM modes (Transverse Magnetic) within the cavity resonator [35]–[38]. Geometrically speaking, the cavity resonators can be classified into pillbox and reentrant cavity monitors [39]. A reentrant cavity monitor provides the advantage of a compact size compared to the pillbox with the added advantage of separation

of the induced electric and magnetic fields within the cavity volume (for the choice of pickup).

The mode of interest for the beam current measurement is the monopole mode i.e., (TM_{010}), which has a maximum of the electric field in the center of the cavity that is proportional to the beam current. The boundary condition of the TM_{010} mode is such that its E-field is terminated on the cavity metallic walls, so for a classical pillbox cavity, the diameter is at least half the wavelength corresponding to the resonance frequency [38], [34].

Similarly, the dipole mode (TM_{110}) of the cavity provides beam position information. The field patterns of the dipole mode are such that only off-centered beams excite it. The dipole mode amplitude is proportional to the bunch charge and beam position offset but without information on the sign of the offset. The sign of the offset is determined by the phase measured with respect to a reference cavity whose TM_{010} resonance frequency is the same as that of the dipole mode cavity i.e., TM_{110} resonance frequency. Thus, for effective position measurement, i.e., information on the bunch offset and its sign, two separate cavities are needed. To achieve position resolution from a cavity BPM in the range of nm, such as in the extraction line of the KEK Accelerator Test Facility (ATF) [38, 39], the amplitude of the TM_{010} mode at the resonance frequency of the TM_{110} mode has to be minimized. Due to the finite quality factor of the cavity and the relatively stronger TM_{010} mode, the frequency separation between the TM_{010} and the TM_{110} mode is recommended to be at least a few 100 MHz to minimize its influence on the measurement.

The cavity monitors' major advantages include their radial symmetry, which allows simple and accurate manufacturing [41], and a lower noise floor compared to its closest competitor, i.e., capacitive monitors, due to its narrowband characteristics. Some of the disadvantages in the functioning of a cavity resonator are, among others, the need for another monitor for calibration and the excitation of the monopole mode at the resonance frequency of the dipole mode in position cavity monitors.

1.8 Aim of the thesis

For beam current and position measurements of the proton beam in the PROSCAN beamlines, the interceptive monitors of the types discussed in section 1.6 offer the service of a watchdog. However, these monitors have issues related, as described in section 1.3. Therefore, to resolve these issues, the use of a non-

interceptive beam current and position monitor is considered. Following a critical analysis of the existing and conventionally used non-interceptive beam diagnostics, the principle of the cavity resonator has been identified as a potential candidate to measure the beam parameters of interest. The required specifications of the cavity resonators are to measure the beam current for proton beams in the range 0.1- 10 nA with a beam current resolution of 50 pA and to measure the beam position with a resolution of 0.50 mm for proton beams with energies of 238-70 MeV.

The objective of the thesis is to report on the performance of the cavity resonators in the beamline as a monitor of both beam current and position. The beam current monitor is a TM_{010} cavity resonator, and the beam position monitor is a TM_{110} cavity resonator, both tuned to 145.7 MHz. This is the second harmonic of the beam repetition rate (i.e., 72.85 MHz) to have a reasonable amplitude of resonance excitation (i.e., measured signal), without considerable RF interference.

1.9 Overview of the Thesis

Chapter 2 shortly presents the theoretical background of an LC resonator as a beam current monitor and its parameters of interest such as quality factors and coupling constant, and formulation of the beam-cavity interaction. Chapter 2 lays the foundation for the Beam Current Monitor (BCM) prototype design with the help of the design code ANSYS High-Frequency Structure Simulator (HFSS). A good agreement between the simulated and the analytical estimate of the pickup signal for a given beam current provides confidence for the design and manufacture of the prototype.

Chapter 3 deals with the experimental characterization of the prototype BCM on a stand-alone test-bench and in the beamline. This Chapter looks into the source of resonance frequency drift in the prototype with the help of S-parameter measurements. Chapter 3 validates the BCM prototype design and its performance for low beam current (0.1-10 nA) in the energy range of 70-230 MeV.

Chapter 4 introduces the principle of a cavity Beam Position Monitor (BPM) working on the dipole mode of excitation from the perspective of a conventional pillbox cavity. Chapter 4 establishes the foundation for the choice of a fourfold dielectric-filled reentrant cavity over the conventional pillbox design. ANSYS HFSS is used to determine the mechanical dimensions of the BPM prototype, whose dipole mode resonance frequency is tuned to 145.7 MHz. The reliability of the design is confirmed with good agreement between the simulated and the analytical estimate of a pickup signal for a given beam offset position.

Chapter 5 characterizes the BPM prototype with measurements on a stand-alone test-bench and in the beamline. The test-bench characterization identifies the deviations in the performance of the BPM prototype in an ideal measurement scenario. Chapter 5 provides the reader with brief information on the source of errors causing these deviations, highlighting the importance of mechanical symmetry of the BPM components and RF isolation. Chapter 5 validates the BPM prototype in the proton beam at two different energies of 138 MeV and 200 MeV, using a simple spectrum analyzer over a current range of 0.1-10 nA and with a position resolution of 0.5 mm. In addition, a new improved BPM design, that is expected to deliver twice better position sensitivity than the prototype is described.

Chapter 6 contains a summary of justifications for our design considerations, measurement observations, and performance of the BCM and the BPM. Chapter 6 ends with the pros and cons of the cavity BCM and BPM designed compared to existing interceptive monitors in the PROSCAN beamline. Chapter 6 concludes the thesis by pointing out the potential for cavity resonators based on future developments in proton therapy.

1.10 Appendix

1TA 1: Key parameters of the COMET cyclotron (latest information) [5]

General Properties	
Type	Isochronous Sector
Extracted energy	250 MeV
Extracted beam current	1000 nA
Extraction efficiency	80%
Number of turns	650
Ion Source	Internal cold cathode
Total weight	90 tons
Outer diameters	3.4 m
Magnetic properties	
Average magnetic field	3.8 T at center
Stored field energy	2.5 MJ
Operating current	160 A
Rated power of cryo coolers	40 kW
RF System	
Frequency	72.85 MHz
Operation	2^{nd} harmonic
Number of dees	4
RF power consumption	300 kW

1.11 References

[1] H. Paganetti, “Proton Beam Therapy,” *Phys. World Discov.*, p. p 1-23, 2017, doi: 10.1088/978-0-7503-1370-4ch1.

[2] M. Schippers, “PSI ’ s SC cyclotron ‘ COMET ’ for proton therapy,” in *PSI-JUAS*, 2012.

[3] M. W. McDonald and M. M. Fitzek, *Proton Therapy at the Paul Scherrer Institute*, vol. 34, no. 4. 2010.

[4] J. M. Schippers *et al.*, “The use of protons in cancer therapy at PSI and related instrumentation,” *J. Phys. Conf. Ser.*, vol. 41, no. 1, pp. 61–71, 2006, doi: 10.1088/1742-6596/41/1/005.

[5] J. T. A. Geisler, C. Baumgarten, A. Hobl, U. Klein, D. Krischel, M. Schillo, “Status Report of the ACCEL 250 MeV Medical Cyclotron,” *Proc. ‘‘Cyclotrons 2004, 17th Int. Conf. Cyclotrons Their Appl.*, no. April 2016, p. 5, 2004, [Online]. Available: http://epaper.kek.jp/c04/data/CYC2004_papers/18A3.pdf.

[6] J. M. Schippers *et al.*, “The SC cyclotron and beam lines of PSI’s new protontherapy facility PROSCAN,” *Nucl. Instruments Methods Phys. Res. Sect. B Beam Interact. with Mater. Atoms*, vol. 261, no. 1-2 SPEC. ISS., pp. 773–776, 2007, doi: 10.1016/j.nimb.2007.04.052.

[7] R. Dölling, “Profile, Current, and Halo Monitors of the PROSCAN Beam Lines,” 2003. doi: 10.1063/1.1831154.

[8] G. Kube, “Specific diagnostics needs for different machines,” in *CERN Accelerator School, Beam Diagnostics*, 2008, pp. 1–64, doi: 10.5170/CERN-2009-005.

[9] R. C. Webber, “Charged particle beam current monitoring tutorial,” in *AIP Conference Proceedings 333*, 2008, vol. 3, no. May 2008, pp. 3–23, doi: 10.1063/1.48014.

[10] B. Tesfamicael *et al.*, “Technical Note: Use of commercial multilayer Faraday cup for offline daily beam range verification at the McLaren Proton Therapy Center,” *Med. Phys.*, vol. 46, no. 2, pp. 1049–1053, 2019, doi: 10.1002/mp.13348.

[11] R. Dölling, “Progress of the Diagnostics At the Proscan Beam Lines,” in *Proceedings of DIPAC*, 2007, pp. 361–363.

[12] R. Dölling, “Beam Diagnostics for Cyclotrons,” in *Vol. 19. Cyclotrons2010 Proceedings*, 2010, pp. 344–350, [Online]. Available:

http://accelconf.web.cern.ch/AccelConf/Cyclotrons2010.

[13] R. Dölling, “Ionization chambers and secondary emission monitors at the PROSCAN beam lines,” in *AIP Conference Proceedings*, 2006, vol. 868, pp. 271–280, doi: 10.1063/1.2401414.

[14] R. Dölling, “Profile, Current, and Halo Monitors of the PROSCAN Beam Lines,” in *AIP Conference Proceedings*, 2004, vol. 732, pp. 244–252, doi: 10.1063/1.1831154.

[15] P. Forck, *Lecture Notes on Beam Instrumentation and Diagnostics*. CreateSpace Independent Publishing Platform, 2015.

[16] M. Gasior, R. Jones, T. Lefevre, and H. Schmickler, “Introduction to Beam Instrumentation,” in *Proceedings of the CAS-CERN Accelerator School: Advanced Accelerator Physics, Trondheim, Norway, 18-29 Aug 2013*, doi: 10.5170/CERN-2014-009.23.

[17] H. Koziol, “Beam diagnostics for accelerators,” in *CAS - CERN Accelerator School : Basic Course on General Accelerator Physics*, 2005, pp. 1–44, doi: 10.5170/CEN-2005-004.154.

[18] B. Instrumentation, “New Parametric Current Transformer.” https://www.bergoz.com/en/npct (accessed Sep. 04, 2020).

[19] P. Heeg, A. Peters, and P. Strehl, “Intensity measurements of slowly extracted heavy ion beams from the SIS,” in *AIP Conference Proceedings 333*, 1995, pp. 287–293, doi: 10.1063/1.48053.

[20] D. Kramer, B. Dehning, E. B. Holzer, and G. Ferioli, “Very high radiation detector for the LHC BLM system based on secondary electron emission,” *IEEE Nucl. Sci. Symp. Conf. Rec.*, vol. 3, no. January, pp. 2327–2330, 2007, doi: 10.1109/NSSMIC.2007.4436611.

[21] J.-C. Denard, “Beam Current Monitors,” in *CAS - CERN Accelerator School: Course on Beam Diagnostics*, 2008, pp. 141–155, doi: 10.5170/CERN-2009-005.

[22] P. Forck, P. Kowina, and D. Liakin, *CERN Accelerator School Beam Diagnostics*. CERN EUROPEAN ORGANIZATION FOR NUCLEAR RESEARCH, 2009.

[23] D. J. Griffiths, *Introduction to Electrodynamics*, vol. 73. 2005.

[24] A. W. Chao, K. H. Mess, M. Tigner, and F. Zimmermann, *Handbook of accelerator physics and engineering, second edition*. Singapore: World Scientific, 2013.

[25] A. Caracappa, C. Danneil, R. Fliller, D. Padrazo, and O. Singh, “A PPS compliant injected charge monitor at NSLS-II,” in *IBIC2016 Proceedings*, pp. 422–425, doi: 10.18429/JACoW-IBIC2016-TUPG37.

[26] F. Stulle, J. Bergoz, W. P. Leemans, and K. Nakamura, “Single pulse sub-picocoulomb charge measured by a turbo-ICT in a laser plasma accelerator,” in *IBIC2016 Proceedings*, pp. 119–122, doi: 10.18429/JACoW-IBIC2016-MOPG35.

[27] C. Jing, J. Shao, J. Power, and C. Yin, “A Low Cost Beam Position Monitor System,” in *IPAC 2018: the ninth International Particle Accelerator Conference*, 2018, pp. 7–9, doi: 10.18429/JACoW-IPAC2018-WEPAF059.

[28] P.Kowina, P.Forck, W. Kaufmann, P.Moritz, F. Wolfheimer, and T. Weiland, “FEM Simulations - A powerful tool for BPM design,” in *Proceedings of DIPAC2009*, 2009, pp. 35–37, [Online]. Available: http://accelconf.web.cern.ch/AccelConf/d09/index.htm.

[29] P. Ausset *et al.*, “First results from the IPHI Beam instrumentation,” in *IBIC2016 Proceedings*, 2018, pp. 413–416, doi: 10.18429/JACoW-IBIC2016-TUPG34.

[30] M. Gasior, “An Inductive Pick-Up for Beam Position and Current Measurements,” in *DIPAC2003 Proceedings*, 2003, no. January 2003, pp. 53–55.

[31] P. Odier, “A New Wide Band Wall Current Monitor,” in *Proceedings of DIPAC 2003*, 2003, no. May, pp. 216–218, [Online]. Available: http://accelconf.web.cern.ch/AccelConf/d03/.

[32] L. Mingtao *et al.*, “APPLICATION OF WCM IN BEAM COMMISSIONING OF RCS IN CSNS,” in *10th International Particle Accelerator Conference*, 2019, pp. 636–638, doi: 10.18429/JACoW-IPAC2019-MOPRB028.

[33] J. Crisp and B. Fellenz, “Tevatron Resistive Wall Current Monitor,” *J. Instrum.*, vol. 6, no. 11, 2011, doi: 10.1088/1748-0221/6/11/T11001.

[34] Y. I. Kim *et al.*, “Cavity beam position monitor system for the Accelerator Test Facility 2,” *Phys. Rev. Spec. Top. - Accel. Beams*, vol. 15, no. 4, pp. 1–16, 2012, doi: 10.1103/PhysRevSTAB.15.042801.

[35] M. Puglisi, “Conventional RF cavity design,” *CAS - Cern Accel. Sch.*, 1992.

[36] R. Feynman, R. Leighton, and M. Sands, “Cavity Resonators,” in *The Feynman lectures on Physics Vol.2: Mainly Electromagnetism and Matter*, vol. II, New York: Basic Books, 2011, pp. 23.1-23.17.

[37] E. Jensen, “RF Cavity Design,” in *CAS - CERN Accelerator School*, 2007, no. 1, pp. 1–73, doi: 10.5170/CERN-2014-009.405.

[38] R. Lorenz, “Cavity beam position monitors,” in *AIP Conference Proceedings 451*, 1998, pp. 53–73, doi: 10.1063/1.57039.

[39] F. Gerigk, “Cavity types,” in *CAS - CERN Accelerator School : RF for accelerators*, 2010, pp. 277–298, doi: 10.5170/CERN-2011-007.277.

[40] S. Walston *et al.*, “Performance of a high resolution cavity beam position monitor system,” *Nucl. Instruments Methods Phys. Res. Sect. A Accel. Spectrometers, Detect. Assoc. Equip.*, vol. 728, pp. 53–58, 2013, doi: 10.1016/j.nima.2013.05.196.

[41] V. Sargsyan, “Comparison of Stripline and Cavity Beam Position Monitors,” 2004.